Non-contact and non-invasive water level measurement outside metal pipes with electromagnetic acoustic resonance

Yingjie Shi[a], Xiaoming Jin[b], Jiahong Jiang[a], Shihui Tian[a], Tairan Lei[a], Morteza Tabatabaeipour[c], Dayi Zhang[d], Ke Xu[a,*]

[a] Collaborative Innovation Center of Steel Technology, University of Science and Technology Beijing, Beijing 100083, China

[b] CGN Inspection Technology Co., Ltd, Suzhou, China, 215000

[c] School of Engineering, Ulster University, Belfast, BT15 1AP, UK

[d] Centre for Ultrasonic Engineering, University of Strathclyde, Glasgow, G1 1XW, UK

Non-contact and non-invasive water level measurement outside metal pipes with electromagnetic acoustic resonance

Abstract: Accurate measurements of water levels within metal pipes are vital, particularly in environments where thick-walled pipes serve as critical components, such as in nuclear facilities. Measuring water levels in pipes becomes more difficult under high temperatures and pressures. In response to this need, a method involving electromagnetic acoustic measurement is proposed. This method begins with a transducer emitting a high-frequency pulse designed for precise measurements of wall thickness, then calculates the resonance frequency using the time intervals between echoes. Finally, the transducer emits an excitation signal at the fundamental resonance frequency to measure the water level. At low water levels, the measurement is conducted by manually scanning along the pipes, utilizing varying energy losses. At high water levels, the resonance echo method is employed. Numerical simulations have demonstrated that this approach effectively improves signal amplitude, thereby ensuring the robustness of the measurement. Experimental results also demonstrated that the proposed method boosted the echo signal-to-noise ratio to approximately 15 dB. Additionally, it successfully detected water levels in both aluminum and stainless-steel pipes. Therefore, it is considered to be a highly efficient non-contact and non-invasive method to measure liquid levels in metal pipes, and it has proved to hold significant potential for engineering applications.

Keywords: Water level measurement; Electromagnetic acoustic transducer; Resonance enhancement; Stainless-steel pipe

1. Introduction

Water level monitoring [1] has widespread and practical applications in various critical fields such as nuclear power plant cooling water pipelines, high-pressure boilers, and chemical water transmission pipelines. The safety and lifespan of equipment are significantly affected by thinned walls [2] and internal water levels.

In pipelines operating under pressurized and sealed conditions, invasive methodologies that could potentially compromise the original structure are generally deemed unacceptable. The

* xuke@ustb.edu.cn; phone 8610 62332159; fax 8610 62332947;

presence of an anti-corrosion layer and elevated temperatures necessitates non-contact detection techniques to prevent corrosion-related complications. Metal surface grinding, which could inadvertently damage the protective layer, and the use of coupling agents [3] are prohibited. Therefore, developing a method to measure the internal water level in thick-walled, sealed metal pipes is both a practical and challenging research question.

Current water level detection methods encompass a broad spectrum, including the capacitive method, floating method [4], optical fiber method [5-8], radar method [9-11], and the ultrasonic method [12]. A comparison of these methods is presented in Table 1, which indicates that ultrasonic methods are the only viable solution in this scenario.

Table 1 Comparison of level measuring methods.

Sensor	Non-invasive	Non-contact	Metal wall	Technology maturity	Pros & Cons
Capacitive	×	×	×	High	Detect all non-metallic targets. Low cost.
Floating gauge	×	×	✓	High	Cannot be used under high pressure situations. Low cost.
Optical fiber	×	×	✓	High	High temperature environment. Expensive.
Radar level gauge	×	✓	✓	High	Excellent performance. Expensive for higher accuracy.
Laser level gauge	×	✓	✓	High	indirect and continuous level measurement. Extreme accuracy.
Piezoelectric ultrasonic	✓	×	✓	High	Coupling agent. Non-metallic/ metallic containers. Low cost.
Electromagnetic acoustic	✓	✓	✓	Medium	Non-invasive, non-contact measurement of liquid level in closed containers. Low cost and strong stability.
Laser ultrasonic	✓	✓	✓	Low	Cannot be used as a receiving transducer. Expensive.
Air-coupled ultrasonic	✓	✓	✓	Low	Greatly affected by the environment. Extremely low transducer efficiency. Unstable.

In ultrasonic liquid level measurement [14], guided waves and bulk waves [15] represent two wave modes that have been extensively researched and applied. Zhang et al. proposed an ultrasonic method for measuring the liquid level in whiskey casks. By utilizing the presence or absence of bulk wave echoes and moving scans, they achieved centimeter-level precision in non-metallic containers [16]. Liu et al. designed a method that falls under the guided wave category [17], where they developed separated electromagnetic acoustic transmitters and receivers with a fixed distance of 350 mm to estimate liquid levels based on differing surface arrival times. Liu et al. proposed a method for measuring liquid levels via the Lamb energy loss, which utilizing the guided wave method for scanning [18].

Considering the differing ultrasonic impedances at solid-liquid and solid-air interfaces, Zhang et al. used a longitudinal wave piezoelectric probe to conduct in-wall echo experiments, distinguishing liquid levels through energy differences during scanning [19]. Dixon et al. proposed a non-contact bulk wave ultrasonic system for measuring liquid levels in thin-walled beverage containers, although specific details of the measurement system were not provided [20]. MacLauchlan et al. have proposed a patented technique for determining the liquid level within a container using an electromagnetic acoustic transducer (EMAT) [21]. This method involves

emitting and receiving longitudinal ultrasonic waves to the thin metal wall or thin metal foil seals of the container with EMAT, and then determining the liquid level by analyzing the flight time of the echo.

The guided wave method is considered inefficient because it depends on scanning, and its measurement accuracy is affected by the size of the probe. Moreover, the existing EMAT bulk wave method is mainly suitable for measuring water levels in metal containers with thin walls. Accurately measuring water levels inside thick-walled metal pipes is of substantial practical significance.

Laser ultrasonics [22], typically employed as transmitting transducers, need to be used in conjunction with other ultrasonic transducers due to their high cost and large size, making practical applications difficult. Air-coupled ultrasonic [23] transducers are easily disturbed by the environment, exhibit poor stability, and lower transducer efficiency. In contrast, EMAT is more cost-effective and stable. There exists promising potential for the application of EMAT in certain scenarios, for example, in the inspection of nuclear power plant pipes.

Despite its advantages, EMAT has its own limitations. Notably, its transduction efficiency is lower than that of piezoelectric ultrasound. In the presence of a magnetic field, the vertical magnetic field induces stronger surface residual magnetism compared to the horizontal field, thereby enhancing the shear wave efficiency of EMAT [24]. However, shear waves are incapable of propagating in liquids [25], necessitating the use of less efficient longitudinal wave transducers. Furthermore, the energy penetration efficiency of EMAT at solid-liquid interfaces is approximately 20 dB lower than that at continuous impedance. This results in an extremely low signal-to-noise ratio (SNR) for an electromagnetic ultrasonic water level measurement system. Conventional EMAT optimization strategies, such as high-power excitation [26][27], weak signal amplification, probe design [28], and matching [29], have reached a rather mature stage with limited room for improvement. In this innovative paper, reliable measurements are realized and ensured by exciting resonant waves.

The analysis underscores the challenges associated with using EMAT for water level measurement, primarily due to its low SNR, which renders EMAT almost infeasible for practical applications. To extend its use, Electromagnetic Ultrasonic Resonance (EMAR) was developed, gaining recognition in recent years. Its applications span various domains, including sheet thickness measurement [30][31], material characterization [32], and detection of composite layer debonding [33]. This advancement enables the application of EMAR in water level measurement for thick-walled pipes, forming the cornerstone of this theoretical framework. However, traditional EMAR [34], which typically excites long pulses and uses frequency sweeps [35], does not require resolution in the time domain and is not entirely suitable for water level measurement, necessitating improvements in this study.

The main contribution of this paper is the proposal of an improved EMAR, which uses EMAT to excite long-period signals, causing acoustic waves to resonate and thereby enhancing signal amplitude. Specifically, the proposed method involves determining echo time intervals through thickness measurement, obtaining resonance frequencies, and enhancing signal amplitude by exciting resonance frequency waves. This approach enables effective water level measurement. Resonance attenuation is employed to distinguish water levels in scenarios of low or no water, while high water levels are calculated by the reception time of the echo reflected from the liquid-air interface.

The theoretical foundation of the proposed water level measurement is established in Section

2, analyzing energy loss along the ultrasonic propagation path and illustrating resonance simulation using Matlab. Section 3 outlines the design of longitudinal wave probes and simulates high water level measurements using the finite element method. Section 4 explains the method for obtaining resonance frequencies and utilizes the echo method for rapid high water level measurements. Experimental results of water levels are presented and discussed in Section 5. Section 6 summarizes the findings and discusses potential avenues for future research.

2. Theoretical analysis

2.1. Energy Loss during ultrasonic propagation

EMAT generates ultrasonic bulk waves. As these waves propagate through solid media, attenuation occurs. This attenuation results from the combined effects of eddy current energy losses, absorption, scattering, and diffraction. The attenuation coefficient in each terms can be written as follows

$$\alpha_E = \alpha_e + \alpha_a + \alpha_s + \alpha_d\,, \tag{1}$$

where α_E is the overall attenuation coefficient, α_e denotes the attenuation due to eddy current losses, α_a signifies the absorption attenuation, α_s corresponds to the scattering attenuation, and α_d represents the attenuation due to diffraction losses.

For a small section of the large diameter pipe, the section can be approximated as a small flat plate to simplify the analysis model [36].The reflection coefficient (R) and transmission coefficient (T) at different medium interfaces [37] can be written as follows

$$R = \frac{W_l - W_s}{W_l + W_s} \qquad T = \frac{2W_s}{W_l + W_s}\,, \tag{2}$$

where W_s and W_l represent the acoustic impedances of solid and liquid, respectively. Given that the energy is directly proportional to the square of the pressure amplitude, the distribution of energy in transmission and reflection is deduced as follows

$$\frac{I_R}{I_I} = \left(\frac{W_l - W_s}{W_l + W_s}\right)^2 \qquad \alpha R = \frac{I_T}{I_I} = \frac{4W_l W_s}{(W_l + W_s)^2}\,, \tag{3}$$

where I_I denotes the intensity of the sound wave prior to reaching the contact interface, and the energy intensities of the reflected and transmitted sound waves are represented by I_R and I_T. α_R is the reflection coefficient. The acoustic impedance, W, is calculated as follows

$$W = \rho c, \tag{4}$$

where ρ is the density, and c is the sound velocity. The parameters are detailed in Table 2, showing that the reflected energy is 70.6% and the transmitted energy is 29.4%. Similarly, the energy reflection at the interface between stainless steel and water is calculated to be 88.0%. Nearly 100% of the energy is reflected at the aluminum-air interface, which is also the case for the water-air interface.

Table 2 Acoustic impedance related parameters.

Symbol	Parameter meaning	Value
ρ_s	Aluminum density	2.7 g/cm^3
c_s	Aluminum longitudinal wave sound velocity	6300 m/sec
ρ_l	Density of water	1 g/cm^3
c_l	Speed of sound in water (25°C)	1480 m/sec

W_s	Acoustic impedance in aluminum	$17.01 * 10^5$ Rayl
W_l	Acoustic impedance in water	$1.48 * 10^5$ Rayl
$\frac{I_R}{I_I}$	Reflected energy from solid to liquid	29.4%
$\frac{I_T}{I_I}$	Transmitted energy from solid to liquid	70.6%

Ultrasonic propagation loss through water can be attributed to several factors, including spreading loss, absorption loss, and boundary loss [38]. Such attenuation losses are approximately 0.002 dB per millimeter [39]. Consequently, when the propagation distance in water in the case of a 200-mm diameter pipe is relatively short, the propagation loss can be considered negligible.

2.2. Signal attenuation in time-domain

The time-domain received signal is the primary source for analyzing water level measurements. Therefore, understanding signal attenuation in time-domain signals is crucial. The signal consists of multiple echoes reflected from the opposite end of the transducer. The relationship between the amplitude A_i of the *i*-th echo signal and the amplitude A_1 of the first echo is represented by the following equation [40].

$$A_i = A_1 {\alpha_R}^i e^{-i\alpha_E T_0} \ (i = 1, 2, 3, \dots N_1) \ , \tag{5}$$

where α_R represents the reflection coefficient, ${\alpha_R}^{\mathrm{i}}$ is the energy loss caused by i liquid-solid interfaces. T_0 is the echo round-trip time at resonance, here we take $T_0 = \frac{1}{\mathrm{f}} = 1.9$ μs. For longitudinal waves, the relaxation time coefficient α_E can be estimated as 7000 [41].

The time-domain expression of the *i*-th echo $A_i(t)$ is as follows, which is a sinusoidal wave truncated by a rectangular window.

$$A_i(t) = \begin{cases} A_i cos(2\ \pi ft) & ((i-1)T_0 \geq t \leq (i+N-1)T_0) \\ 0 & \left(t < (i-1)T_0 \ or \ t > (i+N-1)T_0\right) \end{cases} . \tag{6}$$

By superimposing the waveforms of Eq. (6), we obtain $A(t)$ in the following equation.

$$A(t) = \sum_{i=1}^{N_1} A_i(t) \ . \tag{7}$$

The parameters of the numerical simulation are shown in Table 3. There, N_1 denotes the number of bottom reflections, the maximum value of which correlates to the length of the time axis discussed later. Considering the constraints of the hardware system and the blind zone, the effective length of the time T_{max} is taken as 132 μs. Therefore, we define N_1 to be an integer equal to or greater than the value of $\left(\frac{T_{max}}{T_0} + 1 - N\right)$, which is 61.

Table 3 Numerical simulation parameters.

Parameter	Value	Parameter	Value
Signal frequency f	525 kHz	Resonance number N_1	61
Amplitude A_1	1 V	Attenuation coefficient α_E	7000
Excitation pulse train period N	10 cycles	Solid–liquid interface energy loss α_R	0.88
The echo round-trip time T_0	1.9 μs	Solid–gas interface energy loss α_R	1

The energy attenuation of the echo is simulated using MATLAB. Fig. 1(a) shows multiple echo signals ($A_i(t)$) at resonance. The echo signals are summed up to obtain the time-domain results A

(t), and the envelope is obtained, as illustrated in Fig. 1(b).

The differences between the curves of the solid-liquid interface and the solid-air interface are significant and merit attention. Here is an example to better demonstrate the difference in amplitude between these curves. At the solid-liquid interface, the peak-to-peak value in the resonant state is 11.5, which is approximately six times greater than in the non-resonant state. In contrast, the peak-to-peak value at the solid-air interface is 19.2, yielding a peak-to-peak ratio of 1.67 when comparing the solid-air interface to the solid-liquid interface. Since energy is proportional to the integral of the amplitude squared, the energy ratio between the solid-air interface and the solid-liquid interface is 2.79. These differences underpin the theoretical basis for employing energy thresholds to distinguish between interfaces, as discussed in Section 5.4.

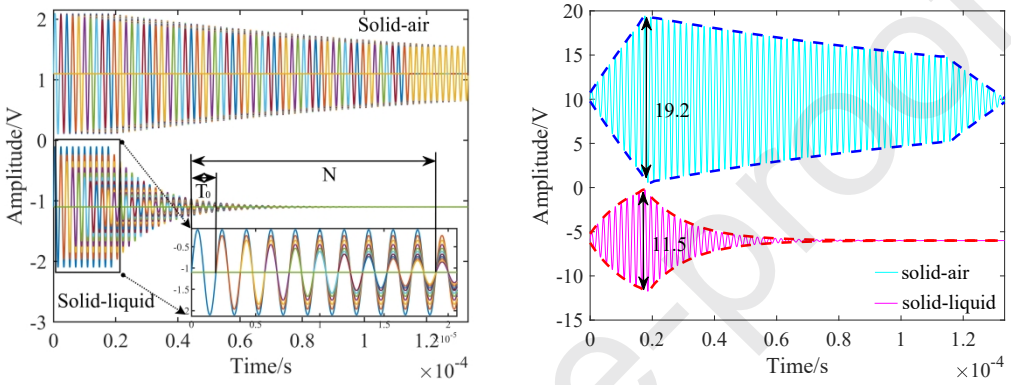

(a) (b)

Fig. 1. Simulation diagram of echo energy attenuation: (a) received resonant echoes at the solid-air interface (top) and at the solid-liquid interface (bottom), (b) signals after superposition and envelope processing.

The above analysis concludes that utilizing the frequency corresponding to wall resonance can increase the received signal amplitude and that the energy at the solid-air interface differs from that at the solid-liquid interface. These findings form the theoretical basis for high and low water level measurements.

3. Transducer design and simulation

3.1. Design of longitudinal wave transducer

As mentioned in the previous section, two types of bulk waves propagate in solids, namely longitudinal waves [42] and shear waves, but only longitudinal waves can propagate in liquids. When the shear wave reaches the solid-liquid interface, it is not transmitted through the interface. Therefore, almost all the energy is reflected back, resulting in no energy loss. The EMAT designed in this study is used to generate ultrasonic longitudinal waves [43][44]. Currently, there are two prevalent methods for generating EMAT longitudinal waves: excitation of alternating current in the coil [45] under the influence of the horizontal magnetic field produced by the electromagnet, and excitation of alternating current [46][47] in the coil in the presence of a horizontal magnetic field between the two poles of the magnet. Despite the pipe possessing a certain degree of curvature, it can be approximated as a flat plate [48] when the ratio of diameter to thickness is substantial [36]. Here, double magnets and cage coils [49][50][51] are employed to ensure that the bottom surface of the magnet is tangentially parallel to the pipe, thereby enhancing the strength of the magnetic field and the efficiency of energy conversion. The schematic diagram and 3D module of the

longitudinal wave transducer are illustrated in Fig. 2(a) and Fig. 2(b), respectively.

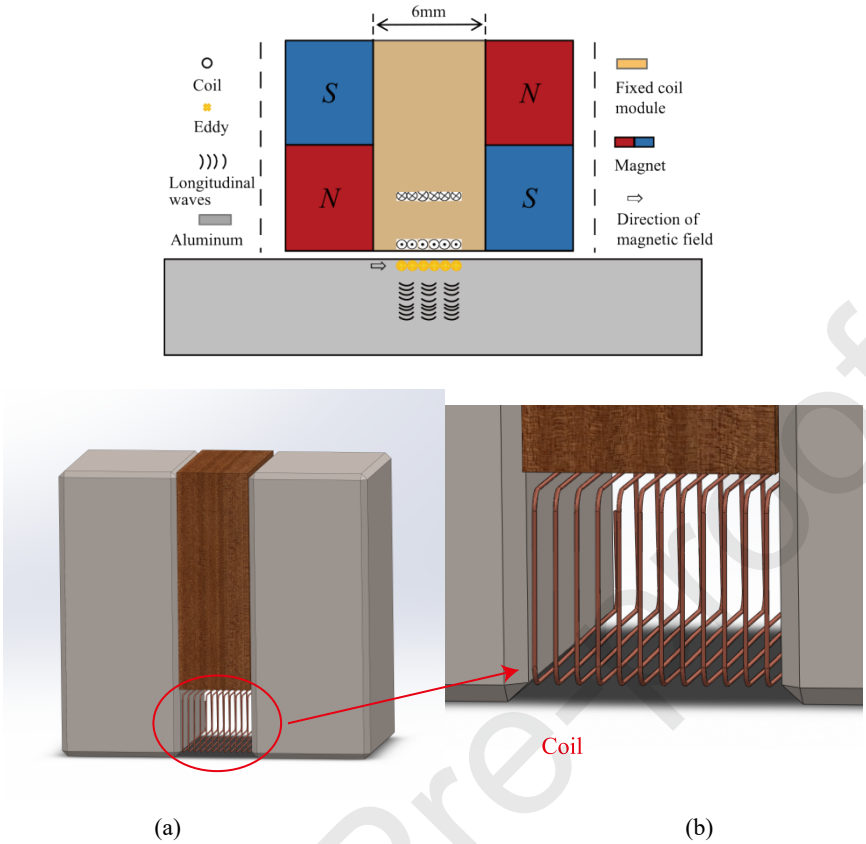

Fig. 2. Longitudinal wave EMAT: (a) schematic representation, (b) fabricated transducer.

The dimensional parameters of the transducer are detailed in Table 4. During the fabrication process, it is essential to completely cover the magnet with copper foil tape to prevent the occurrence of echoes within the magnet. Additionally, the coils are encased in tape to protect against potential collisions with metal and to enhance their resistance to wear.

Table 4 Parameters of the transducer.

Parameter	Value
Magnet size	20×30×50 mm^3
Magnet spacing	6 mm
Coil diameter	0.2 mm
Coil turns	20
Upper and lower coil distance	8 mm

There is a negative exponential relationship between the received voltage and the lift-off distance [52], making it essential to keep a small lift-off distance. In the following experiments, the transducer uses multiple layers of tape to achieve a lift-off distance of approximately 0.5 mm and is placed on the surface of the pipe. At this point, the air gap is very small or considered non-existent. It is important to note that for the EMAT used in this study, a lift-off distance of less than 0.5 mm is necessary. A larger lift-off will result in an extremely low SNR, making it impossible to measure the water level.

3.2. Finite element simulation

Figure 3 illustrates the EMAT water level detection model used in this study, simulated using COMSOL Multiphysics. The model captures the interactions among solid mechanics, static and alternating magnetic fields, and pressure acoustics. The components include an air domain, a permanent magnet, a coil for generating pulsed eddy currents, an aluminum plate, and water. The vertical magnetic field strength above the magnet is 1 T, and the lift-off distance between the magnet and the aluminum plate is 0.5 mm. Resonance is induced by exciting a three-cycle wave at 525 kHz on a 6 mm thick aluminum plate. The sound wave is then transmitted into the water, with the waveform amplitude increasing due to the resonance effect.

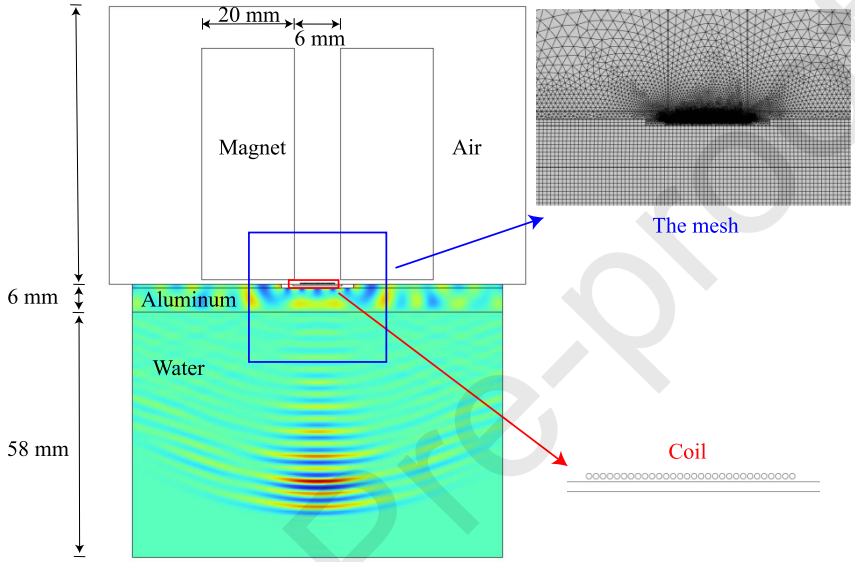

Fig. 3. Acoustic field simulation result under resonance condition. The excitation waveform is a three-cycle 525 kHz wave, and the simulation time is 31.5 μs.

A 2D model is employed to streamline the simulation process, optimizing computational efficiency by reducing the volume of calculations and minimizing temporary data storage requirements. In this model, the size parameters are consistent with the actual probe, thereby enhancing the fidelity. To ensure accuracy, the minimum mesh size in the simulation corresponds to 1/5 of the skin layer thickness. Given the simulation duration of 200 μs, managing extensive data within a single computation necessitates high computational resources. Therefore, the simulation is divided into two phases, with the second phase commencing immediately after the first iteration concludes. The simulation's time step is configured to 1/10 of the period. These considerations are crucial for achieving successful simulation outcomes.

Fig. 4 presents the voltage within the coil. The first echo aligns with the waveform envelope in the numerical simulation depicted in Fig. 1, matches the theory. However, due to the propagation distance and multi-interface reflection issues, the secondary echo is heavily attenuated, reducing its amplitude similar to the noise level. This diminishes the resolution. The signal prior to 67 μs exhibits a significant DC offset. To reduce visual clipping, the signal remains unchanged. Instead, only the subsequent signal is amplified by 100 dB and then concatenated with the preceding data.

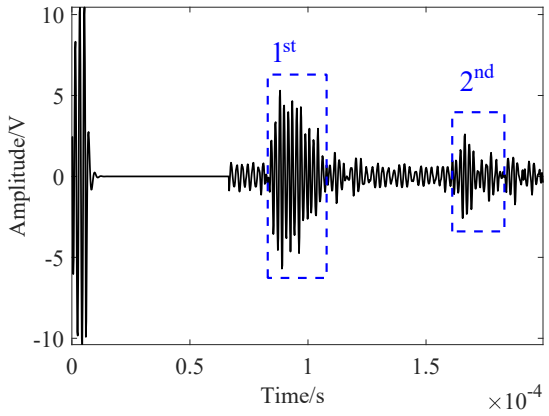

Fig. 4. A typical simulated RF signal received by EMAT.

4. Fast resonance method for measuring water level

4.1. Resonance frequency calculation and measurement process

Initially, a high-frequency pulse is generated to gauge wall thickness. Subsequently, the resonant frequency is determined from the echo time, facilitating the measurement of water level using resonant waves.

The thickness *d* is expressed as

$$\begin{cases} d = c_p * \frac{t}{2} \\ t = \sum_{i=1}^{N} \Delta t_i \,/N \; (i = 1,2,3,\ldots N) \end{cases}, \tag{8}$$

where t is the average of multiple echoes interval time. Δt_i represents the time difference between the i-th and (i-1)-th echoes, and N represents the total number of valid echoes. The equation to calculate longitudinal wave wavelength λ_p is

$$\lambda_p = \frac{c_p}{f}, \tag{9}$$

$$\lambda_p = \frac{2d}{M}(M = 1,2,3,\ldots)\,. \tag{10}$$

Eq. (9) indicates that the wavelength equals the ratio of sound velocity c_p to frequency f. Eq. (10) indicates the relationship between thickness, wavelength, and wave number M, which is the number of cycles observed in a interval [32].

Based on the Eq. (8)–Eq. (10), the resonance frequency f is expressed as follows

$$f = \frac{c_p * M}{2d} = \frac{M}{t} = \frac{M}{\sum \Delta t_i / N}(M = 1,2,3,\ldots)(i = 1,2,3,\ldots N)\,. \tag{11}$$

The water level measurement approach is structured as follows: Initially, a three-cycle 4 MHz wave is employed for thickness measurements. After a 20 ms interval, the resonant excitation frequency (e.g., 525 kHz) is transmitted. The waveform schematic for this excitation is illustrated in Fig. 5. Compared to the pulse used for thickness measurement, the resonant wave excitation uses a higher amplitude, leading to improved conversion efficiency.

According to Eq. (11), the resonance frequency is determined based on the echo of time from the thickness measurement. Despite variations in metal materials, pipe curvature, or temperature, the resonance frequency for water measurement remains consistent. This design ensures efficient

and real-time resonance-based water level measurement without the need for frequency scanning.

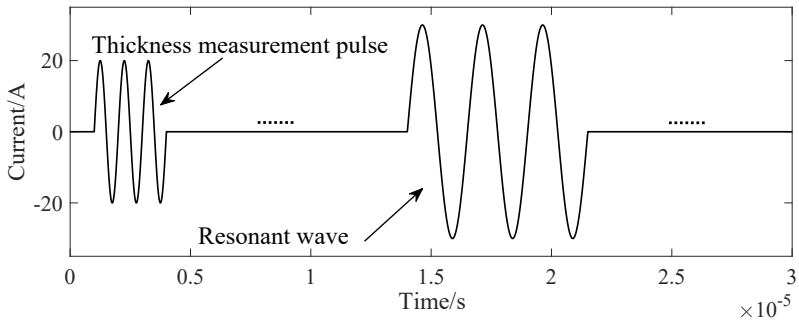

Fig. 5. Thickness measurement-resonance excitation waveform.

4.2. Ultrasonic time-of-flight at high water level

When the water level is high, echo method is employed. Ultrasonic longitudinal waves are generated at the bottom of the pipe wall, subsequently traversing through the pipe wall, the solid-liquid interface, and the water. Upon reaching the liquid-air interface, the waves undergo reflection. These reflected waves propagate along the reverse path, ultimately reaching the outer surface of the pipe wall, where they are then converted into electrical signals by the transducer. The entire process is illustrated in Fig. 6. The water level d_w is expressed as follow

$$d_w = \frac{c_w * (t_1 - t_2 - t_3 - \frac{2d_s}{c_s})}{2}. \tag{12}$$

In the Eq. (12), d_s represents the thickness of the pipe wall, c_s denotes the longitudinal wave velocity in the solid, $\frac{2d_s}{c_s}$ stands for the round-trip propagation time. c_w is the velocity of sound in water. The initiation command is sent to the equipment, and the time until the reception of the first valid peak of the echo is denoted as t_1.

While the system initiates waveform transmission, it starts the analog-to-digital conversion (ADC). However, due to the gate time of the RITEC power amplifier, the ADC starts collecting data earlier than the output pulse, which constitutes the main part of t_2. During the simulation, t_2 is zero.

Taking the superposition of resonance into account, we define t_3 to be the effective commencement time of the theoretical emission. This is typically characterized as the time of the second emission peak.

In the experiment, we calibrated the sum of t_2 and t_3 using a standard water level gauge. This calibration process reduces bias errors, for example in converting time of flight to water column height. The parameters mentioned above are listed in the table below.

Table 5 Time parameters of two types of pipes

Parameter	Aluminum pipe value	Stainless-steel pipe value
$t_2 + t_3$	7.86 μs	5.78 μs
d_s	6 mm	5 mm
c_s	6300 m/s	5900 m/s
c_w	1500 m/s	1500 m/s

Fig. 6 is a schematic diagram illustrating Eq. (12), aiming to visually depict the calculation method for high water level and the meaning of each parameter.

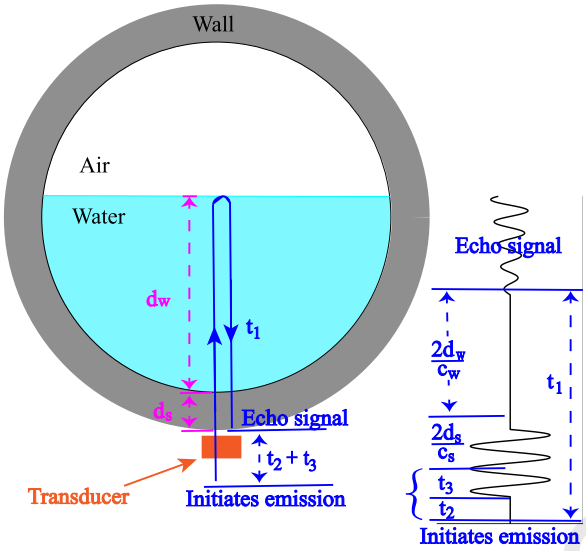

Fig. 6. Schematic of high-water level echo calculation.

5. Experiment

5.1. Experimental setup

The instrumental setup, as depicted in Fig. 7, comprises a self-developed ZYNQ7020 board, a power amplifier, a weak signal amplifier, a duplexer, an EMAT probe, and a PC. At the core of the experimental setup is the ZYNQ7020 board, a specialized circuit designed around a heterogeneous FPGA. This board generates TTL gate and sine signals through the DAC902 and utilizes the AD9226 for sampling with a refresh rate of 50 MHz. The entire system operates on a Linux platform running Jupyter and employs Python for programming. It controls the transmission of signals to the transducer through a power amplifier while concurrently capturing the incoming analog echo signals. The Ga2500 power amplifier can deliver up to 5 kW of power output. Additionally, the signal amplifier, specifically RITEC's BR640A, comes equipped with a hardware filter ranging from 100 kHz to 3 MHz and offers a gain of 48 dB. The system also includes a duplexer, the RDX-EM2, which provides an estimated preamplifier gain of 20 dB. Connectivity between the PC and the ZYNQ7020 board is facilitated via WiFi, allowing for control over the experimental setup. An oscilloscope is integral to the setup for signal monitoring. A self-made cage coil and a transducer fitted with a rectangular magnet are horizontally positioned at the base of the pipe, approximately 0.5 mm above it.

This experiment utilizes two types of test samples: one is a stainless-steel pipe measuring 200 mm in diameter, 1000 mm in length, and 5 mm in thickness, while the other is an aluminum pipe with dimensions of 300 mm in diameter, 1000 mm in length, and 6 mm in thickness. Both ends of each pipe are meticulously sealed using acrylic plates and waterproof adhesive, followed by the addition of water within the pipe. The resonance-based water level measurement experiments are designed to be comprehensive and are conducted across a range of water levels to ensure accuracy and reliability in the findings. By systematically varying the water levels, the experiments can observe and record the measurement accuracy under different conditions.

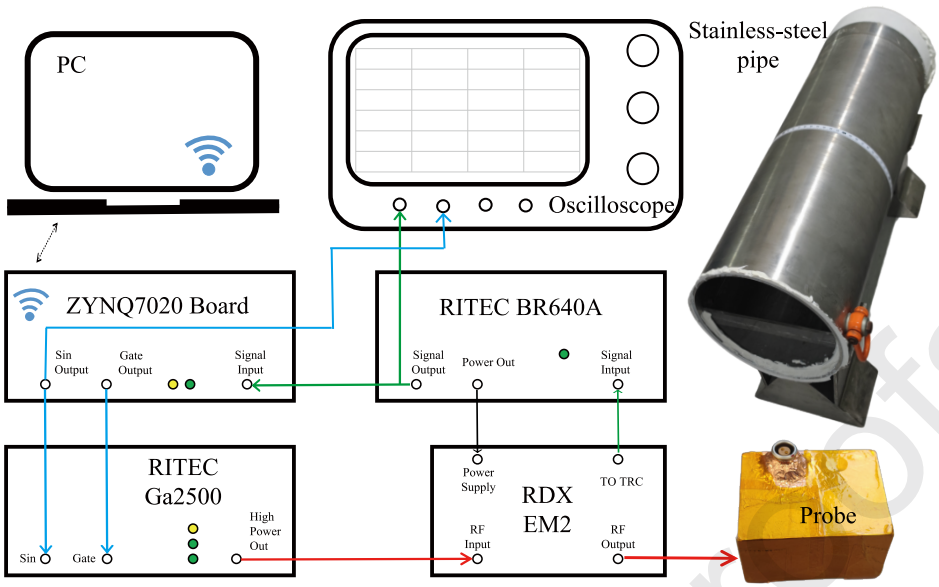

Fig. 7. Experimental equipment and tested pipe.

The measurement points for the transducer, as referenced in the subsequent discussion, correspond to four distinct positions labeled A through D, as illustrated in Fig. 8. Positions C, B, and A represent the interfaces for solid-liquid, solid-liquid (air), and solid-air measurements, respectively, under conditions of low water levels. Conversely, position D is located at the bottom of the pipe, used for the echo method at high water levels.

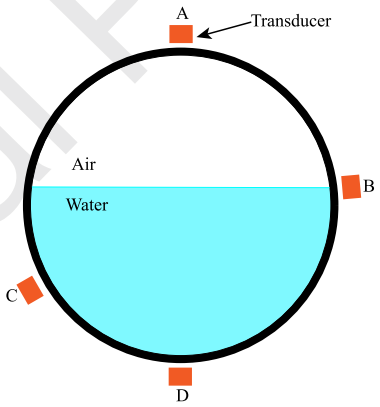

Fig. 8. Different transducer positions for measuring the water level.

5.2. Effect of resonance and nonresonance on echo intensity

An ideal method of measuring water level is to excite a pulse wave, and the wall thickness and water level can be obtained by analyzing the echo time of the pipe wall and the liquid–gas interface. However, the experiment reveals that the water-air interface reflected echo cannot be obtained under conventional high-frequency pulse excitation, primarily due to two factors: the low efficiency of interface transmission and weak EMAT transduction.

From a theoretical standpoint, resonance can enhance the energy of sound waves [53]. Upon substituting the values of $M = 1$, $c_p = 6300$ m/s, and $d = 0.006$ m into Eq. (11), we ascertain that $f = 525$ kHz. When $M = 0.5$, the echo cancellation frequency $f = 262$ kHz. When $M = 2$, the resonance fundamental frequency $f = 1050$ kHz. In addition, we choose approximately the mid-

frequencies of 400 kHz and 700 kHz from the ranges of 262~525 kHz and 525~1050 kHz, respectively. These frequencies are used for comparison with resonant and non-resonant conditions, enhancing the robustness of our analysis. The excitation voltage, power amplifier, and preamplifier remain consistent across all experiments, as do the number of excitation waveforms and the settings for both software and hardware filters.

The experimental results, as depicted in Fig. 9, reveal that echo results cannot be obtained at frequencies of 262 and 700 kHz. At 400 kHz, the echo characteristics are less discernible, and it is difficult to calculate the starting point algorithmically. At 525 kHz, the amplitude and characteristics of the echo signal are most pronounced, enabling the calculation of the water level height. Therefore, it can be concluded that the resonant fundamental frequency serves as the optimal excitation frequency for this method.

The oscillation observed in the low-frequency waveform, as depicted in the figure, is attributed to the application of a band-pass filter. This filter serves to eliminate the oscillation within the blind zone, which is induced by a portion of the emission. In order to accentuate the echo signal, the amplitude of the oscillation within the emission blind zone (prior to 64 microseconds, Fig. 9(c) Blue dotted line) is diminished, as illustrated in Fig. 9. This adjustment allows for a more pronounced representation of the echo signal.

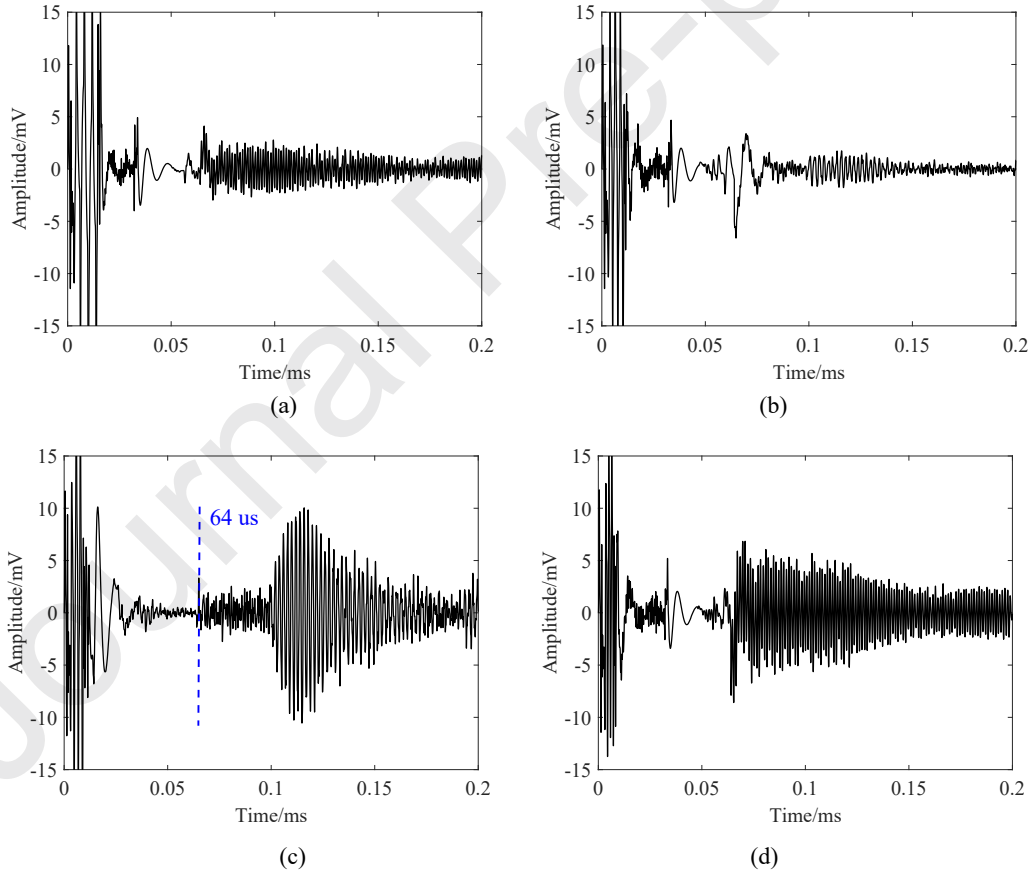

Fig. 9. Resonant/nonresonant echo signals at (a) 262 kHz, (b) 400 kHz, (c) 525 kHz, (d) 700 kHz.

5.3. Effect of resonance frequency doubling on echo intensity

In the experiment, a water level height of 94 mm was measured for the aluminum pipe. The resonance fundamental frequency, calculated based on the echo time difference, was found to be 525 kHz. To ensure the consistency of the emitted pulse width with the energy, a three-cycle wave

was excited at the resonant fundamental frequency, while six and nine cycles were excited at the second and third multiplied frequencies, respectively.

As depicted in Fig. 10(a), the initial 32 μs represents the resonance excitation and its oscillation blind zone. This duration cannot be shortened due to the inherent limitations of the electronic system and excitation frequency. At the 42 μs, the first echo of the bulk wave, excited by the coil above the magnet, is observed. This effect can be mitigated by wrapping copper foil around the magnet. At 136 μs, the resonant wave propagates from the solid to the water, reflects off the liquid-air interface, and ultimately returns to the solid's outer surface where it is detected by the EMAT.

In Fig. 10, a fifth-order bandpass Butterworth filter, with a frequency range of 0.2-5 MHz, is employed to eliminate the bias voltage and suppress the noise's high-frequency components. A comparative analysis of Fig. 10(a)-(c) reveal a slower resonance attenuation of the pipe wall in the latter two figures, resulting in a larger signal amplitude within the 40-100 μs timeframe. However, at 1050 kHz and 1575 kHz, the echo amplitude at the water-air interface is relatively small, leading to a low SNR. The low SNR primarily arises due to two factors: (1) the rate of ultrasound attenuation in water increases with the frequency under the same sound source level. (2) the hardware configurations, including impedance matching and filters, are skewed towards low frequencies. While they can encompass the entire frequency band, their performance is more effective at lower frequencies. The discrepancy is approximately 20% – 30%, but it is not the predominant factor.

Upon comparative analysis, Fig. 10(a) emerges as the most effective, indicating that the resonance fundamental frequency experiences less propagation loss in water and exhibits a shorter resonance energy duration in metals. Consequently, the fundamental frequency is selected for resonance echo-based water level measurement.

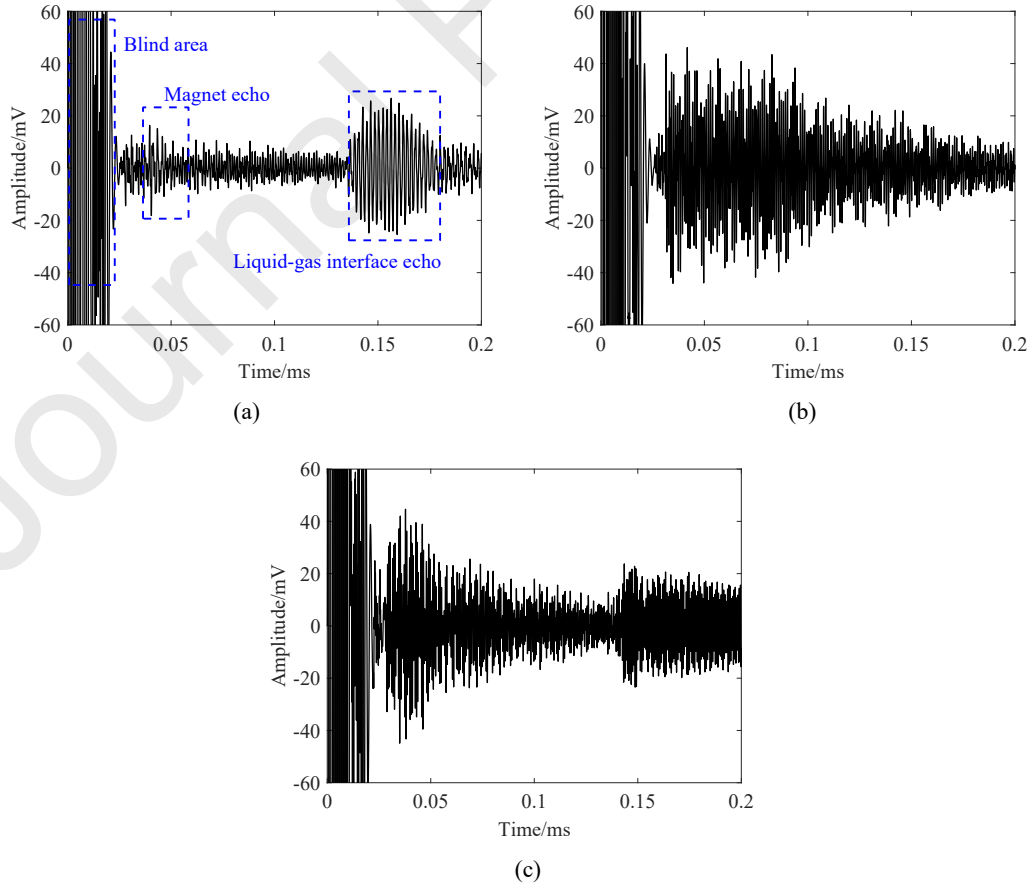

(a) (b)

(c)

Fig. 10. Resonant frequency echo effect at (a) 525 kHz, (b) 1050 kHz, (c) 1575 kHz.

5.4. Analysis of low water results

In the actual experiment, an oscillation blind zone [54] is observed in the electronic system. When the water level is low, the echo falls in the blind zone and the water level cannot be measured. Fig. 11 shows the echo can still be distinguished when the water level is 28 mm, but this is already a more extreme situation. The blue frame is the blind area, and a stronger waveform after that is the magnet echo. Given multiple reflections in the water and the exceptionally long resonance transmission to the water, overlapping in time is easy, thus it is difficult to determine the echo time at the water-air interface.

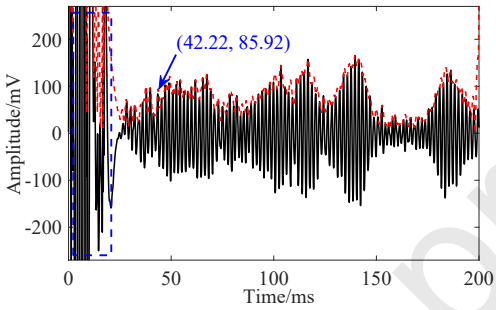

Fig. 11. A typical signal when the water level is low (28 mm).

Given the above situation, resonance analysis is performed at C (solid-liquid), B (the interface of water and air), and A (solid-air) in Fig. 8. At this time, the attenuation is faster when the ultrasonic resonance wave is propagated to water, and slower when it is not transmitted to water (Section 2.2). The analysis time is 81.92 μs (2048 points) after 50 μs (system blind zone), the echo waveforms are shown in Fig. 12(a)-(c). The time domain shows the attenuation is very slow in the anhydrous position, and the oscillation attenuation can hardly be seen in the water area and semi-water area. Spectrum analysis of this segment of data is shown in Fig. 13(a)-(c). By analyzing the energy intensity at 525 kHz, the peak values are 0.55 mV, 1.21 mV, and 7.78 mV. These results indicate the ease of determining the presence of water at the detection point through scanning. The presence of water at the test point can be ascertained based on a threshold value of 4 mV, which is half the amplitude observed at the top in the absence of water.

The frequency domain analysis reveals a line spectrum at 840 kHz, likely due to the switching frequency of equipment in the laboratory's computer room or another source. When the frequency corresponding to the pipe thickness is close to the ambient EMI spectrum, it affects the analysis of resonance attenuation. In such cases, selecting multiple of the fundamental resonance frequency could be a viable solution. While this aspect is not explored in the present study, it holds potential for enhancing the stability of the water measurement system.

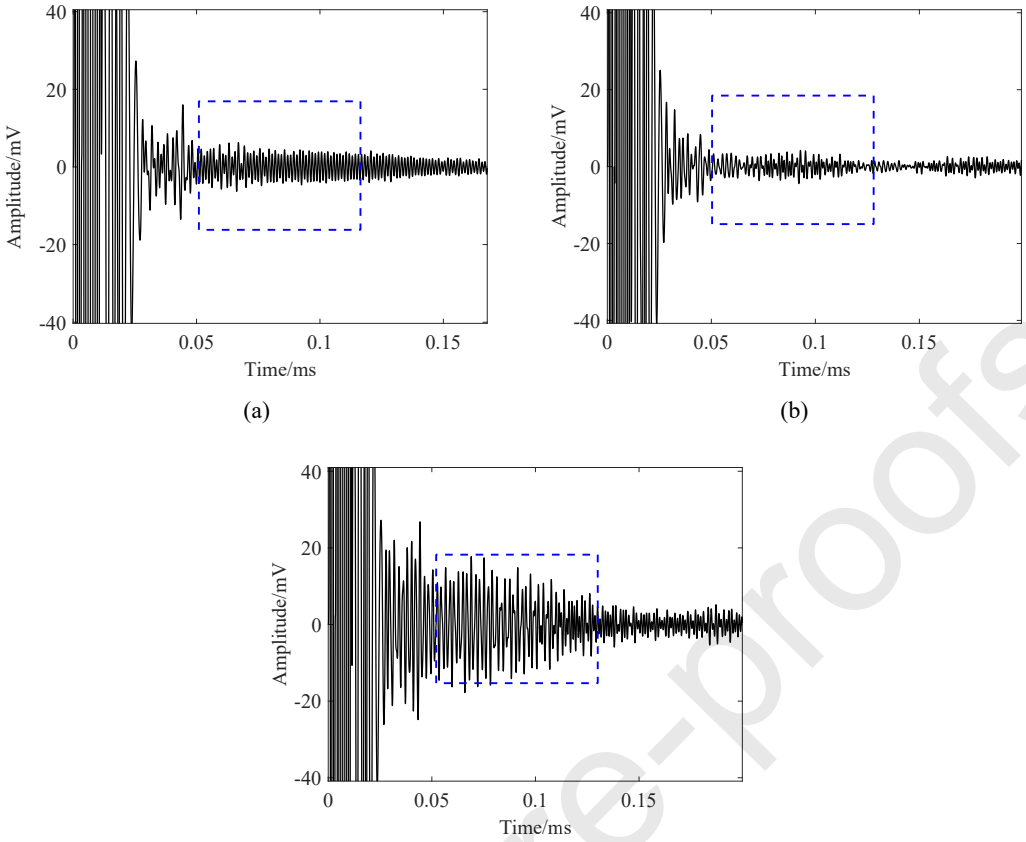

Fig. 12. Time domain analysis of resonance attenuation, which is conducted at (a) C, (b) B, (c) A.

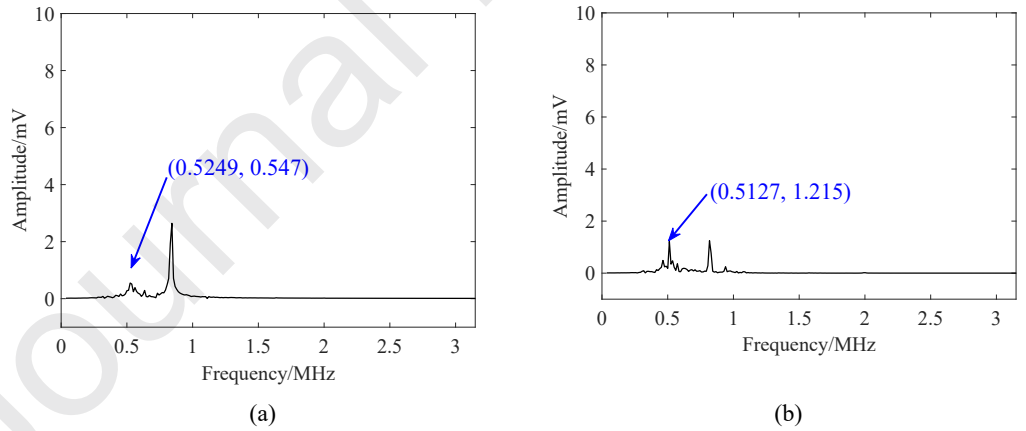

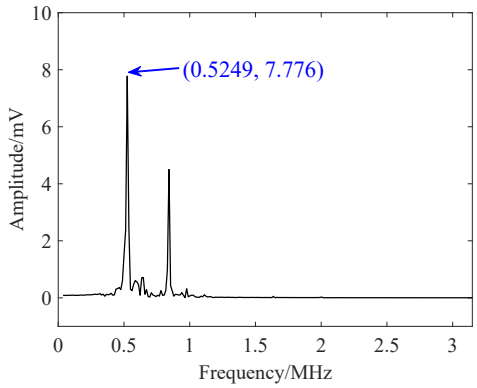

(c)

Fig. 13. Frequency domain analysis of resonance attenuation, which is conducted at (a) C, (b) B, (c) A.

As shown in Fig. 14, a manual scan is conducted on the aluminum pipe. This scanning procedure systematically covers the pipe's circumference from -120 mm to 120 mm, with 10 mm intervals. The outcomes of this scan are illustrated in Fig. 15. A threshold of 5 mV is utilized for segmentation purposes, and the solid-liquid interfaces at -78 mm and 77 mm are denoted as w_1 and w_2, respectively. In this equation, d represents the inner radius of the pipe, which measures 144 mm. The water level h_1, computed by Eq. (13), is determined to be 20.36 mm. It's consistent with the actual value of 20.0 mm.

$$h_1 = d * (1 - cos(\frac{w_1 + w_2}{2\pi d} * 180)) . \quad (13)$$

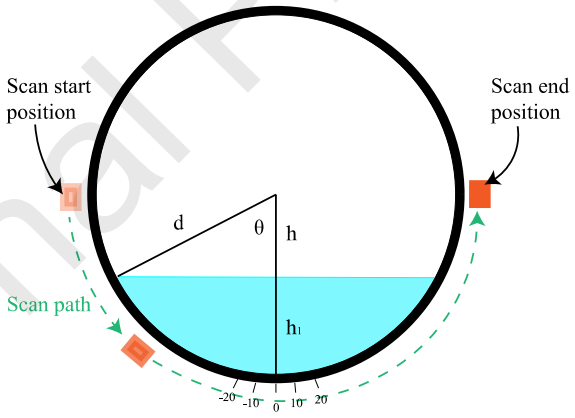

Fig. 14. Low water level circumferential scanning diagram.

While the scanning method proves effective in distinguishing the water level interface, the calculation of the water level height necessitates knowledge of the pipe diameter. An enhancement in signal amplitude is observed at the bottom of the figure, see Fig. 15. This amplitude rise is attributed to the echo reflected by the horizontal water surface falling within the analysis time, resulting in a signal amplification compared to oblique incidence.

In the experiment, the low water level measurement was conducted manually. Measures to reduce the error are to be part of future works, including a reduced scanning interval, narrowed coils, and machine scanning.

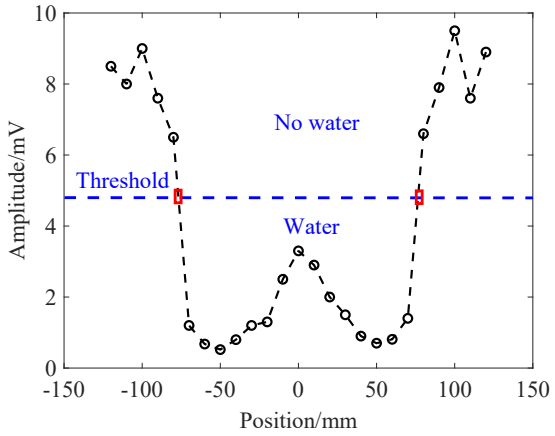

Fig. 15. Low water level circumferential scanning results.

5.5. Experimental results of high water level

Utilizing the experimental conclusions in Section 5.2 and Section 5.3, the resonance fundamental frequency is used for excitation at high water levels. The overall scheme uses the method in Section 4, that is, the resonance frequency is calculated by using the echo time interval after thickness measurement, and a three-cycle sine wave is excited at this frequency. This scheme can adaptively resonate and excite pipes with different thicknesses, and complete the work of thickness measurement and water level measurement in a brief period, which is also one of the main innovations of this paper.

Fig. 16(a)-(b) present the echo results of the water level for aluminum and stainless-steel pipes, respectively, at varying water levels. A comparative analysis reveals that the aluminum pipe exhibits superior performance in terms of noise level and SNR compared to the stainless-steel pipe.

As shown in Fig. 16(c) at a water level of 56 mm, 20 μs prior to the echo start point was selected as noise, and 20 us after the echo start point as signal. Using MATLAB *snr* function, a value of 19.85 dB was obtained. The same method was applied to the other five sets, and their SNR results averaged to approximately 15 dB. It is important to note that the 15 dB SNR was obtained under the specific conditions of our experimental environment. Factors such as electromagnetic interference, probe's lift-off distance, and temperature can affect the SNR.

In the Fig. 16, 0 - 32 μs data is attenuated by 20 dB, thus there is an amplitude change that manifests as an echo-like pattern at the blue dotted line. This operation primarily targets the large amplitude oscillation area induced by the duplexer, where the signal amplitude is substantial, thereby hindering the observation of subsequent signals. This procedure bears resemblance to the process of normalization.

Fig. 16(c) is an enlarged view of the 56 mm primary echo in Fig. 16(a). The rising slope of the envelope first increases and then decreases, and the falling slope also increases first and then decreases. This result is consistent with the red line in Fig. 1(b) of the numerical simulation results.

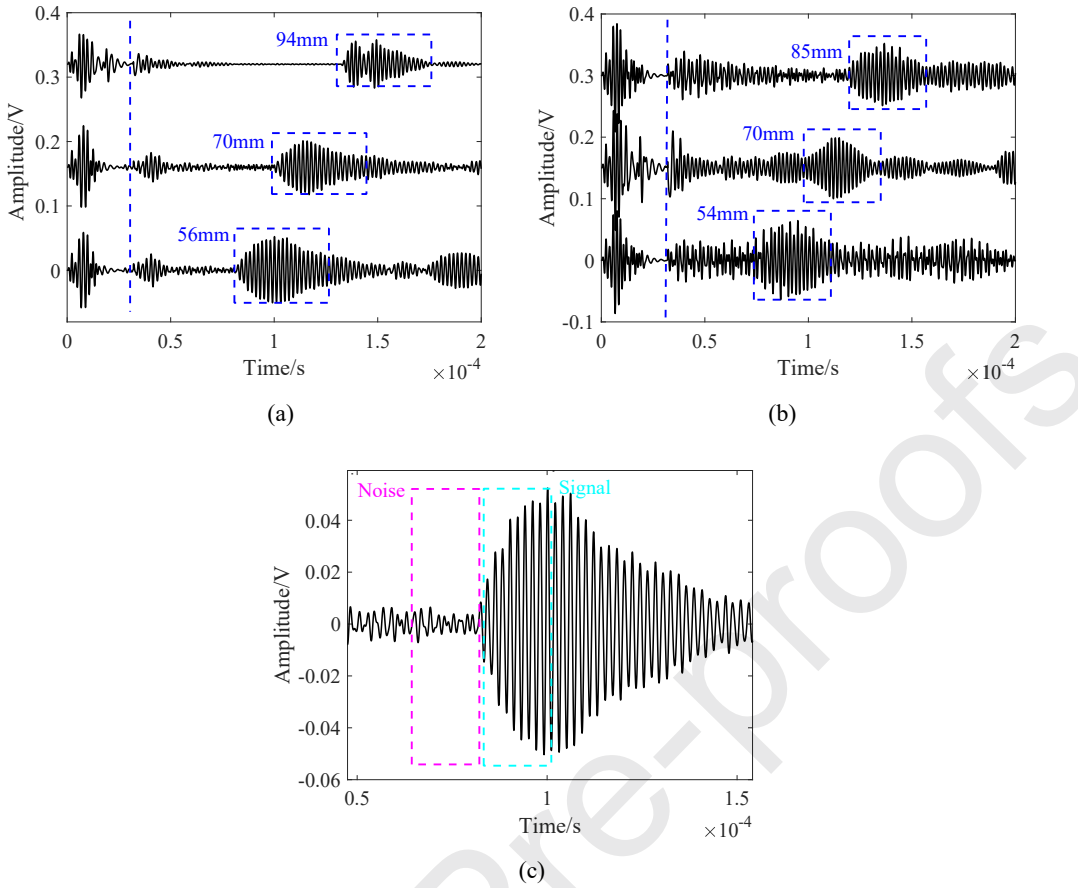

Fig. 16. Resonance water echo diagram: (a) the aluminum pipe, (b) the stainless-steel pipe, (c) enlarged diagram of the primary echo signal.

Using Fig. 16(a) as an example, when the ground truth level is 56.0 mm, $t_1 = 84.3$ μs. By substituting t_1 and the variable values from Table 5 into Eq. (12), the measured level is 55.9 mm. The experimental results are listed in Table 6. The ground truth level is measured using a caliper to measure the water level from the side of the pipe, which has a piece of acrylic to visually confirm the actual level. The measured ground truth values are listed under the "Actual Water Level" column in Table 6. The measured values using the presented method in this paper are marked as “Measured water level”. The absolute errors are the differences between the measured values and the ground truths.

Table 6 Results of water level measurement

Pipe material	Actual water level (mm)	Echo time t1(μs)	Measured water level (mm)	Absolute Error (mm)
Aluminum pipe	56.0	84.3	55.9	0.1
	70.0	103.9	70.6	0.6
	94.0	135.6	94.4	0.4
Stainless-steel pipe	54.0	78.4	53.2	0.8
	70.0	99.6	69.1	0.9
	85.0	121.6	85.6	0.6

5.6. Measurement uncertainty of high water level

The uncertainty in water level measurement is caused by various factors, including the electronic system, temperature variations, and the Time Delay Estimation (TDE). The error introduced by the electronic system is compensated by the t_2 parameter in Eq. (12). To ensure the stability of the water temperature, tap water is left indoors for 24 hours before the experiment. A vernier caliper is used to mark the water level line. A spirit level is placed above the stainless-steel pipe to ensure the water level is horizontal. Measurements are taken 10 times at 30.0, 38.0, 46.0, 54.0, 62.0, 70.0, 78.0, 85.0, and 93.0 mm, respectively. In each measurement, the probe was manually lifted and repositioned back to its original location. The measurement error is shown in Fig. 17.

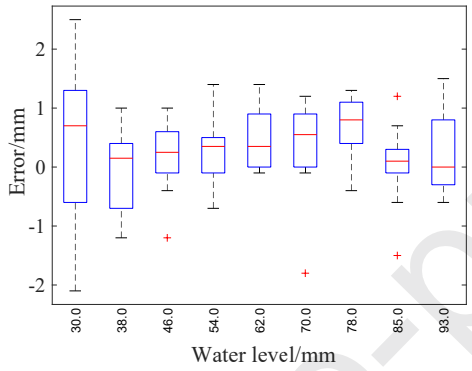

Fig. 17. Measurement error.

As illustrated in the above figure, the median error across various water levels consistently remains within ±1.0 mm. The error is larger at the lower water level (30.0 mm). When the water level is greater than 30.0 mm, the outliers of the error are all within ±2.0 mm, and the maximum and minimum values are within ±1.5 mm. These findings provide substantial validation for the efficacy and precision of the employed measurement technique.

Additionally, materials such as stainless steel, which are characterized by their low electrical conductivity and inability to be magnetized, there are inherent challenges when used in common pipes due to their low transduction efficiency. Consequently, the measurement error associated with such pipes is anticipated to be greater than that observed with carbon steel pipes. Therefore, it is crucial to optimize the probe, particularly from the angles of magnetic circuit design and the application of magnetostrictive force, to mitigate these issues.

6. Conclusion and future work

This paper introduces a novel non-contact and non-invasive technique using electromagnetic acoustic resonance to gauge water levels in metallic pipes, particularly those with thick walls. For lower water levels, an external EMAT performs a circumferential scan along the pipe, utilizing differences in acoustic impedance to determine the liquid's upper boundary. At higher water levels, the fluid level is determined by measuring the duration of resonance echoes.

Originally designed for measuring cooling pipelines in nuclear power plants, this method also shows promise for application in industries using extensive metal piping, such as global chemical logistics.

The study also investigates the impact of signal strength variations from non-resonance, fundamental resonance frequency, and double resonance frequency, concluding that the

fundamental resonance frequency offers the optimal signal for water level measurement.

The efficiency and accuracy of EMAT for these measurements may be affected by factors like the probe's footprint, pipe diameter, and the pipe's inclination angle. Custom EMAT designs that conform closely to the pipe's surface may be required for smaller diameter pipes. Using a gyroscope placed on the probe to measure the pipe inclination angle and compensate for errors is indeed meaningful.

Future research directions include exploring the effects of high temperatures on measurements, estimating and compensating for sound velocity changes under such conditions using thermometers. Developing automatic methods to switch between high and low water level measurements is also a critical area for future study, potentially involving statistical analyses of SNR, errors factors. Additionally, investigating the use of automated scanning robots or fixed-position probes for low water level measurements in radioactive environments is worth exploring.

References

[1] P. Mohindru, Development of liquid level measurement technology: A review, Flow Measurement and Instrumentation 89 (2023). https://doi.org/10.1016/j.flowmeasinst.2022.102295.

[2] G. Diguet, H. Miyauchi, S. Takeda, T. Uchimoto, N. Mary, T. Takagi, H. Abe, EMAR monitoring system applied to the thickness reduction of carbon steel in a corrosive environment, Materials and Corrosion 73 (2022) 658–668. https://doi.org/10.1002/maco.202112915.

[3] W. Gao, W. Liu, Y. Hu, J. Wang, A Novel NaCl Concentration Detection Method Based on Ultrasonic Impedance Method, IEEE Trans Ultrason Ferroelectr Freq Control 68 (2021) 3226–3233. https://doi.org/10.1109/TUFFC.2021.3083773.

[4] S.W. Wang, C.C. Chen, C.M. Wu, A continuous water-level sensor based on load cell and floating pipe, 2018 IEEE International Conference on Applied System Invention (ICASI). IEEE, 2018.

[5] N. Jing, Liquid level measurement based on multi-S-bend plastic optical fiber, Sensor Review 39 (2019) 522–524. https://doi.org/10.1108/SR-08-2018-0199.

[6] J. Ge, X. Cheng, C. Zhao, K. Gui, W. Zhang, F.A. Cheikh, L. Ye, Reflected Light Intensity-Modulated Continuous Liquid Level Sensor Based on Oblique End Face Coupling Optical Fibers, IEEE Sens J 20 (2020) 4229–4236. https://doi.org/10.1109/JSEN.2019.2962610.

[7] W. Wang, F. Li, Large-range liquid level sensor based on an optical fibre extrinsic Fabry-Perot interferometer, Opt Lasers Eng 52 (2014) 201–205. https://doi.org/10.1016/j.optlaseng.2013.06.009.

[8] A.G. Leal-Junior, C. Marques, A. Frizera, M.J. Pontes, Multi-interface level in oil tanks and applications of optical fiber sensors, Optical Fiber Technology 40 (2018) 82–92. https://doi.org/10.1016/j.yofte.2017.11.006.

[9] J.D. Loftis, D. Forrest, S. Katragadda, K. Spencer, T. Organski, C. Nguyen, S. Rhee, StormSense: A New Integrated Network of IoT Water Level Sensors in the Smart Cities of Hampton Roads, VA, n.d. http://www.vims.edu/test/dlm/slrc/index.php.

[10] V. Melnikov, V. Ivanov, I. Teplyashin, M. Timonin, Development and study of a microwave reflex-radar level gauge of the nuclear reactor coolant, Nuclear Energy and Technology 4 (2018) 185–190. https://doi.org/10.3897/nucet.4.31857.

[11] B.T. Sivaprakasam, C. V. Krishnamurthy, K. Arunachalam, Design and Demonstration of a RADAR Gauge for In-Situ Level Measurement in Furnace, IEEE Sens J 18 (2018) 4081–4088.

https://doi.org/10.1109/JSEN.2018.2816016.
[12] W. Gao, W. Liu, Y. Hu, J. Wang, Study of ultrasonic near-field region in ultrasonic liquid-level monitoring system, Micromachines (Basel) 11 (2020). https://doi.org/10.3390/MI11080763.
[13] S. Uhlig, I. Alkhasli, F. Schubert, C. Tschöpe, M. Wolff, A review of synthetic and augmented training data for machine learning in ultrasonic non-destructive evaluation, Ultrasonics 134 (2023). https://doi.org/10.1016/j.ultras.2023.107041.
[14] B. Praher, G. Steinbichler, Ultrasound-based measurement of liquid-layer thickness: A novel time-domain approach, Mech Syst Signal Process 82 (2017) 166–177. https://doi.org/10.1016/j.ymssp.2016.05.016.
[15] J.L. Zhang, Y.L. Shan, Research on ultrasonic liquid level non-contact measurement in sealed vessel, Piezoelectric Acoustooptics 133 (2009): 366-370.
[16] D. Zhang, W. Jackson, G. Dobie, C. Macleod, A. Gachagan, Innovative non-invasive ultrasound method for whisky cask liquid level measurement, Measurement (Lond) 228 (2024). https://doi.org/10.1016/j.measurement.2024.114345.
[17] F. Liu, J. Li, J. Long, L. Xu, Y. Xie, A novel liquid-level measurement method based on electromagnetic acoustic guided waves, in: Conference Record - IEEE Instrumentation and Measurement Technology Conference, Institute of Electrical and Electronics Engineers Inc., 2023. https://doi.org/10.1109/I2MTC53148.2023.10175983.
[18] Y. Liu, X.P. He, T.T. Zhang, B. Li, Liquid-level measurement based on out-of-plane energy of Lamb waves, Applied Acoustics 210 (2023). https://doi.org/10.1016/j.apacoust.2023.109421.
[19] B. Zhang, Y.J. Wei, W.Y. Liu, Y.J. Zhang, Z. Yao, L.H. Zhao, J.J. Xiong, A liquid level measurement technique outside a sealed metal container based on ultrasonic impedance and echo energy, Sensors (Switzerland) 17 (2017). https://doi.org/10.3390/s17010185.
[20] S. Dixon, C. Edwards, S.B. Palmer, Noncontact ultrasonic liquid-level measurement of drink cans, In Process Control and Sensors for Manufacturing II (Vol. 3589, pp. 52-57). SPIE. https://doi.org/10.1117/12.339969.
[21] D.T. MacLauchlan, Method for determining liquid level in a container using an electromagnetic acoustic transducer (EMAT), U.S. Patent 6,176,132, issued January 23, 2001.
[22] H. Kim, B. Balagopal, S. Kerrigan, N. Garcia, M.Y. Chow, M. Bourham, T. Fang, X. Jiang, Noninvasive liquid level sensing with laser generated ultrasonic waves, Ultrasonics 130 (2023). https://doi.org/10.1016/j.ultras.2023.106926.
[23] B. Han, C. Jiang, A.M. Omer, K.O. Hamad, T. Shao, L. He, X. Ding, H. Zhang, J. Fu, J. Meng, Y. Duan, A generic time-frequency analysis-based signal processing and imaging approach for air-coupled ultrasonic testing, NDT and E International 144 (2024). https://doi.org/10.1016/j.ndteint.2024.103101.
[24] S.E. Burrows, Y. Fan, S. Dixon, High temperature thickness measurements of stainless steel and low carbon steel using electromagnetic acoustic transducers, NDT and E International 68 (2014) 73–77. https://doi.org/10.1016/j.ndteint.2014.07.009.
[25] K. Rieger, D. Erni, D. Rueter, Noncontact reception of ultrasound from soft magnetic mild steel with zero applied bias field EMATs, NDT and E International 125 (2022). https://doi.org/10.1016/j.ndteint.2021.102569.
[26] K. Rieger, D. Erni, D. Rueter, Examination of the Liquid Volume Inside Metal Tanks Using Noncontact EMATs from Outside, IEEE Trans Ultrason Ferroelectr Freq Control 68 (2021) 1314–1327. https://doi.org/10.1109/TUFFC.2020.3022946.

[27] H. Bin Jo, S.H. Song, S.H. Lee, H.J. Ryoo, MOSFET Gate Driver Circuit Design for High Repetitive (200 kHz) High Voltage (10 kV) Solid-State Pulsed-Power Modulator, IEEE Trans Power Electron 36 (2021) 10461–10469. https://doi.org/10.1109/TPEL.2021.3062612.
[28] X. Jia, O. Qi, X. Zhang, An improved design of the spiral-coil EMAT for enhancing the signal amplitude, Sensors (Switzerland) 17 (2017). https://doi.org/10.3390/s17051106.
[29] J.P.T. Andrade, P.L.F.C. Bazan, V.S. Medeiros, A.C. Kubrusly, A Simplified One-Parallel-Element Automatic Impedance-Matching Network Applied to Electromagnetic Acoustic Transducers Driving, Automation 4 (2023) 378–395. https://doi.org/10.3390/automation4040022.
[30] R. Urayama, T. Takagi, T. Uchimoto, Online monitoring of pipe wall thinning by electromagnetic acoustic resonance method, E-Journal of Advanced Maintenance 5 (2013).
[31] N. Yusa, H. Song, D. Iwata, T. Uchimoto, T. Takagi, M. Moroi, Probabilistic evaluation of EMAR signals to evaluate pipe wall thickness and its application to pipe wall thinning management, NDT and E International 122 (2021). https://doi.org/10.1016/j.ndteint.2021.102475.
[32] M. Hirao, H. Ogi, Electromagnetic acoustic resonance and materials characterization, Ultrasonics, 35 (1997), 413-421.
[33] T. Liu, C. Pei, X. Cheng, H. Zhou, P. Xiao, Z. Chen, Adhesive debonding inspection with a small EMAT in resonant mode, NDT and E International 98 (2018) 110–116. https://doi.org/10.1016/j.ndteint.2018.05.005.
[34] Z. Cai, Y. Sun, Z. Lu, Q. Zhao, Research on Identification and Detection of Aluminum Plate Thickness Step Change Based on Electromagnetic Acoustic Resonance, Magnetochemistry 9 (2023). https://doi.org/10.3390/magnetochemistry9030086.
[35] M. Yoshida, T. Asano, A New Method to Measure the Oxide Layer Thickness on Steels Using Electromagnetic Acoustic Resonance, Journal of nondestrctive evaluation, 22 (2003): 11-21.
[36] P. Wilcox, M. Lowe, P. Cawley, Omnidirectional guided wave inspection of large metallic plate structures using an EMAT array, IEEE transactions on ultrasonics, ferroelectrics, and frequency control 52, no. 4 (2005): 653-665.
Omnidirectional Guided Wave Inspection of Large Metallic Plate Structures Using an EMAT Array, 2005.
[37] J.L. Rose, P.B. Nagy, Ultrasonic Waves in Solid Media, J Acoust Soc Am 107 (2000) 1807–1808. https://doi.org/10.1121/1.428552.
[38] T.G. Leighton, Fundamentals of underwater acoustics, In Fundamentals of noise and vibration, pp. 373-444. CRC Press, 2003.
[39] L. Xavier, An introduction to underwater acoustics: principles and applications, Springer Science & Business Media, 2002.
[40] M. Hirao, H. Ogi, Electromagnetic Acoustic Transducers: Noncontacting Ultrasonic Measurements using EMATs, Springer Japan (2017). https://doi.org/10.1007/978-4-431-56036-4.
[41] H. Ogi, M. Hirao, T. Honda, H. Fukuoka, Absolute measurement of ultrasonic attenuation by electromagnetic acoustic resonance, Review of Progress in Quantitative Nondestructive Evaluation: Volume 14 (1995): 1601-1608.
[42] W. Shi, Y. Tong, C. Lu, Y. Chen, G. Shen, G. Zeng, Improving laser-EMAT ultrasonic energy conversion efficiency using surface constraint mechanism, Ultrasonics 124 (2022). https://doi.org/10.1016/j.ultras.2022.106729.
[43] G. Zhai, B. Liang, X. Li, Y. Ge, High-temperature EMAT with double-coil configuration generates shear and longitudinal wave modes in paramagnetic steel, NDT & E International, 125

(2022). https://doi.org/10.1016/j.ndteint.2021.102572.
[44] S.H. Lee, S.H. Song, H.J. Ryoo, Current-Loop Gate-Driving Circuit for Solid-State Marx Modulator with Fast-Rising Nanosecond Pulses, IEEE Trans Power Electron 36 (2021) 8953–8961. https://doi.org/10.1109/TPEL.2021.3051041.
[45] N. Pei, B. Zhao, L.J. Bond, C. Xu, Analysis of the directivity of longitudinal waves based on double-fold coil phased EMAT, Ultrasonics 125 (2022). https://doi.org/10.1016/j.ultras.2022.106788.
[46] W. Zhang, Y. Wu, Y. Wu, Z. Cai, An improved design of lamb wave EMAT for A0 wave generation and enhancement, Jpn J Appl Phys 60 (2021). https://doi.org/10.35848/1347-4065/abe641.
[47] H. Liu, T. Liu, Y. Li, Y. Liu, X. Zhang, Y. Wang, S. Gao, Uniaxial stress in-situ measurement using EMAT shear and longitudinal waves: Transducer design and experiments, Applied Acoustics 175 (2021). https://doi.org/10.1016/j.apacoust.2020.107781.
[48] L.M. Martinho, A.C. Kubrusly, L. Kang, J.P. Von Der Weid, S. Dixon, Numerical investigation of unidirectional generation of circumferential SH waves applied to defect detection in pipe, in: IEEE International Ultrasonics Symposium, IUS, IEEE Computer Society, 2022. https://doi.org/10.1109/IUS54386.2022.9958876.
[49] J. Zhang, Z.H. Dong, X. Bin Wang, W.Z. Shi, X. Wang, Q. Tang, Study on characteristics of radiation sound field of line-focusing angled SV wave EMAT, in: Proceedings of 2020 IEEE Far East NDT New Technology and Application Forum, FENDT 2020, Institute of Electrical and Electronics Engineers Inc., 2020: pp. 125–129. https://doi.org/10.1109/FENDT50467.2020.9337541.
[50] J. Zhang, M. Liu, X. Jia, R. Gao, Numerical Study and Optimal Design of the Butterfly Coil EMAT for Signal Amplitude Enhancement, Sensors 22 (2022). https://doi.org/10.3390/s22134985.
[51] S. Wang, Z. Li, L. Kang, Modeling and comparison of three bulk wave EMATs, In IECON 2011-37th Annual Conference of the IEEE Industrial Electronics Society, (pp. 2645-2650). IEEE 2011.
[52] D. MacLauchlan, S. Clark, B. Cox, Recent advancements in the application of EMATs to NDE, In 16th World Conference on NDT, pp. 1154-1161. 2004.
[53] D.I. Bolef, J.G. Miller, High-frequency continuous wave ultrasonics., In Physical Acoustics, vol. 8, pp. 95-201. Academic Press, 1971.
[54] J. Ureña, M. Mazo, J.J. García, A. Jiménez, Reduction of blind zone in ultrasonic transmitter/receiver transducers´Alvaro transducers´ transducers´Alvaro, Sensors and Actuators A 133 (2007) 96–103. https://doi.org/10.1016/j.sna.2006.03.008´A.

Highlights:

1) The resonance method enhances the SNR, enabling more accurate high water level measurements in the time domain.
2) The fundamental resonance frequency is the best excitation frequency for measuring water level.
3) The scanning EMAR method for low water level can effectively reduce the blind spot caused

by the resonance echo method.

Declaration of interests

☒ The authors declare that they have no known competing financial interests or personal relationships that could have appeared to influence the work reported in this paper.

☐ The authors declare the following financial interests/personal relationships which may be considered as potential competing interests: